RSC Advances

PAPER

View Article Online
View Journal | View Issue

Cite this: *RSC Adv.*, 2025, **15**, 14767

Fluorescent silver hydrosol for the dual fluorometric sensing of gallic acid and Cd^{2+}

Mamta Sahu, Mainak Ganguly * and Priyanka Sharma

Received 3rd February 2025
Accepted 23rd April 2025

DOI: 10.1039/d5ra00788g

rsc.li/rsc-advances

Herein, silver-enhanced fluorescence was obtained using a small molecule of salicylaldehyde (SL) in an alkaline solution in the presence of silver nitrate. Ag^{+} was reduced to Ag^{0}, while SL was oxidized to the quinone form OSL. OSL was a very weak fluorophore and exhibited metal-enhanced fluorescence (MEF) in the presence of proximal silver nanoparticle surfaces. MEF was selectively quenched by gallic acid and restored by Cd^{2+}. Thus, a dual-sensing platform was obtained for gallic acid [limit of detection (LOD) = 1.77×10^{-5} M; linear detection range = 10^{-8} to 5×10^{-5} M)] and Cd^{2+} (LOD = 2.4×10^{-6} M; linear detection range = 5×10^{-8} to 10^{-6} M) in a one-pot. The observed lightning rod effect and higher radiative decay rate were ascribed to MEF, while replacing the capping agents was responsible for the tuning of MEF. The sensing protocol was applied to natural samples from real sample sources, and satisfactory results were obtained.

Introduction

Nowadays, the use of fluorescence spectroscopy is almost ubiquitous in life sciences, with diverse applications, such as in the identification of chemical or biological analytes or species.[1,2] Intensive research has been conducted on biosensor platforms that generate amplified fluorescence signals. In these platforms, metallic nanostructures and metallic colloidal nanoparticles are effectively used for enhancing the optical properties of fluorophores. They can interact with proximal fluorophores and generate an enhanced quantum yield with improved photostability at an optimal distance of 5–90 nm. MEF is the term used to describe this phenomenon[3–6]

Pawar *et al.*[7] showed that when AuNP was bonded with physiologically significant Zn^{2+}, it induced MEF from the modified bipyridine-based construct 4-(pyridine-2-yl)-3*H*-pyrrolo[2,3-*c*]quinoline (PPQ). This effect was utilized in a biocompatible bilayer vesicle platform in aquatic settings. When compared with the fluorescence intensity without AuNPs, MEF was visible in the presence of AuNPs when PPQ was bonded with Zn^{2+} to form a complex. Fluorescence enhancement was seen across the three AuNPs utilized in this study with an average diameter of 33 nm, while no enhancement was seen for the AuNPs sized 18 and 160 nm. An *et al.*[8] used the "seed growth" method to synthesize AgNPs of various sizes and the wet oxidation method to create carbon dots (CDs). A straightforward hybrid glass slide-silver nanoparticle-carbon dot (GS-AgNP-CD) structure was employed to successfully detect the MEF effect. To examine the impact of altering the metal group's particle size and the distance between the particles and the fluorophore on the MEF effect, this structure was used to vary the sizes of the AgNPs and the distance between the AgNPs and CDs. The fluorescence improvements of fluorescein attached to various-sized silver colloids were investigated by Lukomska *et al.*[9] They reported the selective binding of thiolated 23-mer oligonucleotide (ssDNA-SH) to silver colloids on quartz slides treated with 3-aminopropyltriethoxysilane (APS). The quantity of fluorescein-labeled complementary oligonucleotide (ssFl-DNA) added was much less than the quantity of unlabelled DNA attached to the colloids. Similar hybridization kinetics were seen on the tiny (30–40 nm) and large (120 nm) colloids, as evidenced by the increase in fluorescence emission. Nonetheless, the sample with large colloids had a final fluorescence intensity that was around 50% greater than the sample with small colloids. Because of its consistent fluorescence signal, the reference sample devoid of ssDNA-SH was utilized to estimate the fluorescence increases of fluorescein attached to the small colloids (E 2.7) and large colloids (E 4.1).

The plasmonic enhancement of the fluorophore 4-(pyridine-2-yl)-3*H*-pyrrolo[2,3-*c*]quinoline (PPQ) and its Zn^{2+} complex caused by gold nanoparticles (AuNPs) was observed in a meticulously constructed bilayer structure of a "niosome", which is a significant class of pharmaceutical nanocarriers composed of nonionic surfactants.[7] Choi *et al.* developed a brand-new proteolytic enzyme nanobiosensor using Au nanoparticles (AuNPs) and a particular peptide sequence (DEVD) that could recognize and cleave caspase-3. The peptide and single-stranded DNA (ssDNA) formed a double bridge between the AuNPs and fluorescein isothiocyanate (FITC), and the short peptide length caused the fluorescence signal to be

Solar Energy Conversion and Nanomaterials Laboratory, Department of Chemistry, Manipal University Jaipur, Dehmi Kalan, Jaipur 303007, Rajasthan, India. E-mail: mainak.ganguly@jaipur.manipal.edu

extinguished. Both the distance and the ability to selectively break down the peptide were enhanced. Following the peptide cleavage procedure, ssDNA was used to keep the Au and the FITC apart. Because the ideal distance of MEF is around 7 to 8 nm, the FITC-ssDNA-AuNP produced a stronger fluorescence signal than the original fluorescence signal from FITC.[10]

Gallic acid (GAc), *i.e.*, 3, 4, 5-trihydroxybenzoic acid, is one of the most frequently encountered phenolic acids in various plants. It is prevalent in multiple plant-based consumables, including leaves, fruits, seeds, tea, and wine,[11,12] and also has applications in sustainable packaging development and food preservation. Food preservation is aided by its antibacterial and antifungal qualities against resistant microorganisms and biofilm formation, its capacity to stop lipid and protein oxidation, and its potential as a color indicator for monitoring food freshness. It provides a method for creating edible packaging by its inclusion into edible polymers. The addition of gallic acid inside a polymer matrix can enhance the packaging capabilities of materials, depending on the dosage and material composition.[13,14]

According to numerous studies, GAc can scavenge free radicals as an antioxidant. GAc may be used as an antioxidant in the human diet, with several research studies showing its anti-carcinogenic, antimutagenic, and anti-oxidative qualities.[15] GAc can have an effect on oxidative stress, the body's molecular oxidation process, which may be prevented or delayed, reducing the risk of illness.[16–19] Furthermore, some human diseases, including diabetes, Parkinson's disease, cancer, Alzheimer's disease, and cardiovascular problems, have been linked to oxidative stress.

One of the most hazardous substances to which humans may be exposed at work or in the environment is cadmium (Cd), a byproduct of the manufacturing of zinc. After absorption, Cd can be effectively stored in the human body, where it can accumulate over a lifetime. The kidney is the primary accumulation location for cadmium, which is particularly harmful to the proximal tubular cells. Through direct bone injury or indirectly through renal failure, cadmium can also result in bone demineralization. Excessive exposure to airborne Cd in the workplace can harm the lung function and raise the risk of lung cancer.[20,21]

In conjunction with zinc, cadmium is a rare but extensively distributed hazardous element that may have detrimental health effects on people involved in various activities or in contact with various materials, including mining, water, smelting, phosphate fertilizers, plating, plastics, Ni–Cd batteries, and pigments. The WHO recommends that the cadmium threshold in drinking water should be no more than 3 $\mu g\ L^{-1}$. Furthermore, it is difficult to remove cadmium from ecological systems since it is not biodegradable. Cadmium buildup in human organs can cause renal problems, bone fractures, and several malignancies. Therefore, identifying this heavy metal ion in biological and environmental samples is a critical issue.[22–26]

In this study, we synthesized fluorescent silver nanoparticles (OSLAg), capped with quinone, for the selective sensing of gallic acid and Cd^{2+} in one pot based on turn-off–turn-on emission.

Experimental section

All the chemicals and reagents utilized in the experiments were analytical grade and were used as received without further purification. All the experiments were performed using triple-distilled water. Following the creation of fresh aqua regia, all the glassware was cleaned using soapy water and copious amounts of distilled water, and was thoroughly dried before use. The silver nitrate was purchased from Sigma-Aldrich. The NaOH was provided by Qualigens and Fisher Scientific, respectively. All the metal salts and salicylaldehyde were supplied by Loba Chemicals. A UV-2600 digital spectrophotometer (Shimadzu) was used to record the UV/vis absorption spectra. A Horiba FluoroMax-4 spectrophotometer was used to analyze the fluorescence at room temperature. The morphology of the particles was examined using a JEOL Make JSM-7610FPlus FESEM system, under high-resolution scanning (1 kV at 1.0 nm, 15 kV at 0.8 nm).

Synthesis of OSLAg

A stock solution of 0.047 M SL was made by dissolving the appropriate amount of SL in 500 mL of 0.005 M NaOH solution. Next, 10 mL of 0.001 M $AgNO_3$ solution, 3 mL of the SL stock solution, and 37 mL of NaOH solution (0.005 M) were mixed thoroughly and aged overnight on the bench at room temperature (30 °C) to obtain the fluorescent hydrosol OSLAg. No stirring was performed during synthesis.

Results and discussion

OSLAg: quinone-capped fluorescent silver hydrosol

SL is an aromatic compound with –OH and –CHO functional groups at the *ortho* position. As SL is insoluble in water, it was dissolved in 0.2 M NaOH to obtain a pale-yellow alkaline SL solution. The introduction of an aqueous $AgNO_3$ solution produced the strongly emissive zero-valent silver hydrosol OSLAg.[27] The phenolates in the SL alkaline solution were transformed to the quinone form during the formation of OSLAg. It was reported that fluorophores sized in between 5–90 nm from metal nanostructure exhibit MEF with a high scattering cross-section and low absorption cross-section.[5,28] Here, the Ag nanoparticles in OSLAg, being in proximity with a weakly fluorescent fluorophore, bestowed it with a higher rate of excitation (lightning rod effect) and a higher rate of emission. Thus, MEF was observed. No external energy was employed in the reaction mixture for the synthesis of OSLAg and the detection of the analytes. Therefore, the process was cost-effective, simple, and energetically convenient.

The optical characteristics of metallic surfaces and particles are varied and intricate. The vibrant hues of noble metal colloids, absorption of surface plasmon resonance of thin metal films, and the quenching of excited fluorophores close to metal surfaces are some examples. Fluorophores' interactions with metal surfaces have recently been exploited to boost the fluorescence intensities of materials, create tests based on gold colloids quenching fluorescence, and to achieve directional

radiation from fluorophores close to thin metal films. It is challenging to forecast whether a certain metal structure—such as a colloid, fractal, or continuous surface—will increase or quench fluorescence in the case of metal-enhanced fluorescence.[24,29,30]

Lakowicz proposed a straightforward theory based on radiating plasmons (RPs) to explain how metals influence fluorescence. The concept is relatively easy to grasp, even if the physics behind it is complicated. The RP model states that the optical characteristics of a metal structure, as determined by electrodynamics, Mie theory, and/or Maxwell equations, may be used to forecast the emission or quenching of a fluorophore close to the metal. For instance, Mie's theory states that the extinction of metal colloids might be caused by either absorption or scattering, depending on the particles' size and shape.[29,31]

Absorption dissipates incident energy, while scattering produces far-field radiation. The RP model predicts that tiny colloids would suppress fluorescence because absorption would outweigh scattering. Conversely, for larger colloids, since the scattering component would outweigh the absorption, larger colloids should improve fluorescence.

Here, OSLAg still demonstrated strong fluorescence (quantum yield = 6.5%, λ_{ex} = 290 nm, λ_{em} = 452 nm) after 8 h aging with alkaline SL and Ag^+. Such 8 h of aging was important for the evolution of fluorescence. SL + Ag^+ without aging could not generate fluorescence. The UV-Vis spectrum of OSLAg showed the appearance of a new peak at 295 nm due to the strong interaction between the quinone and silver in OSLAg (Fig. 1).

The nanoparticle formation was further gauged by zeta potential and dynamic light scattering (DLS) analyses. The zeta

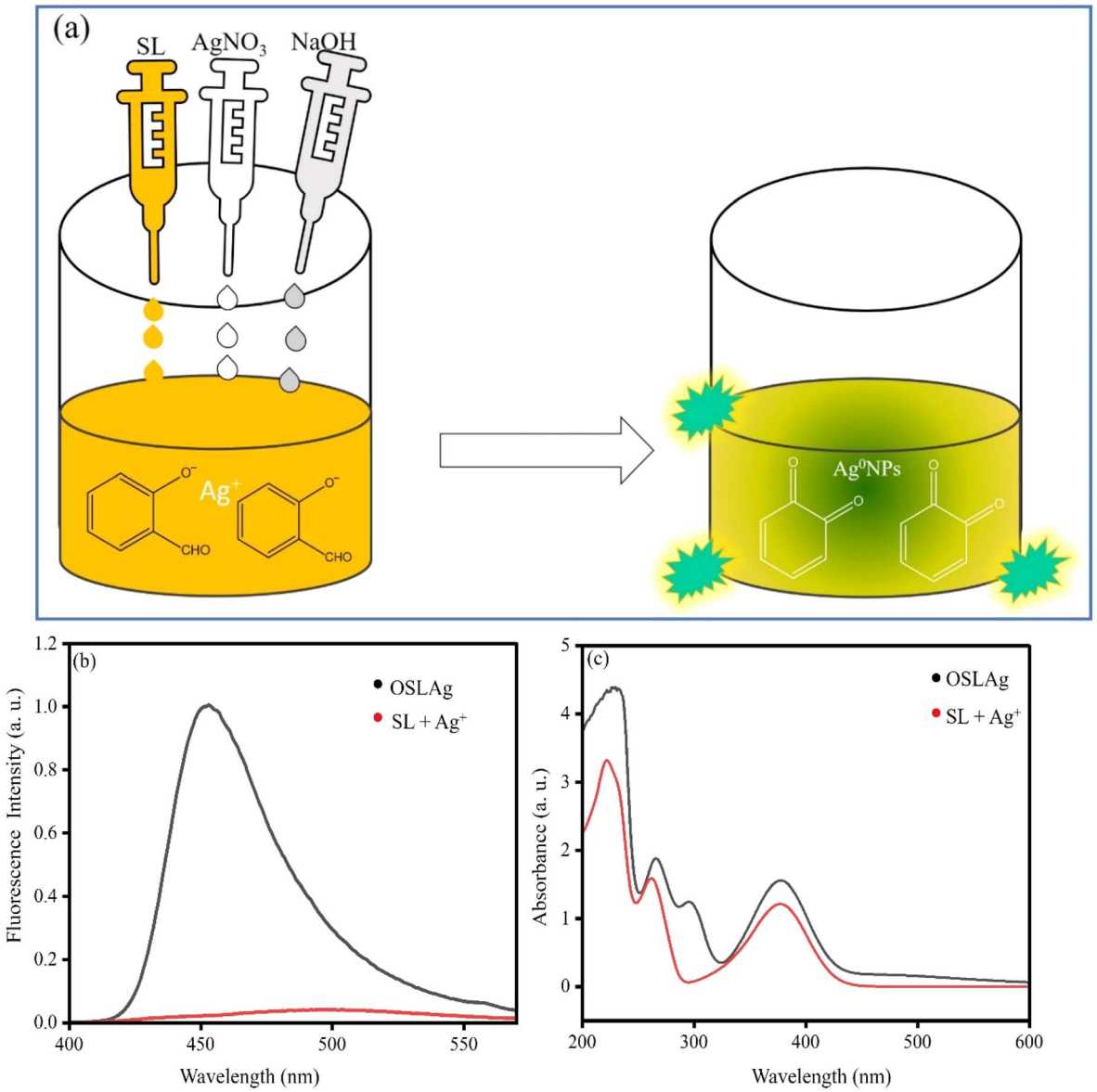

Fig. 1 (a) Schematic representation of the formation of silver nanoparticles. (b) Fluorescence spectra and (c) absorption spectra before and after the formation of OSLAg.

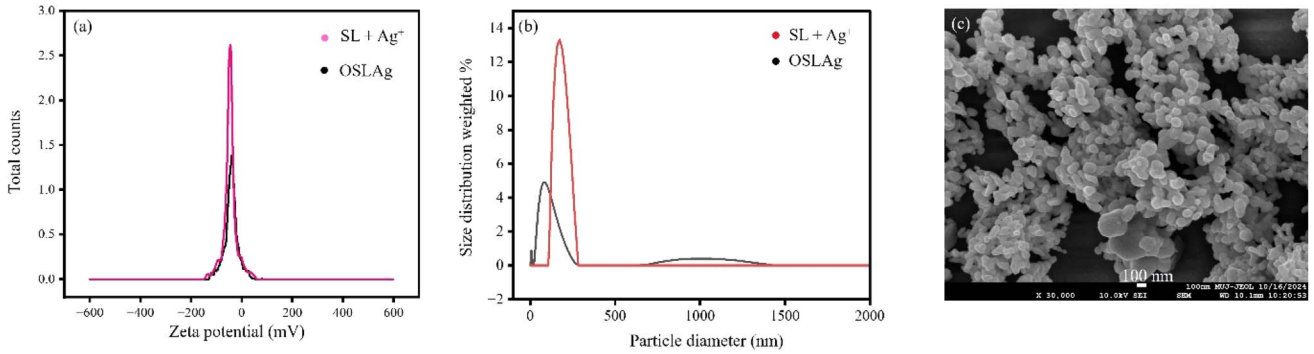

Fig. 2 (a) Zeta potential and (b) DLS plots of OSLAg before and after the formation of OSLAg *via* aging. (c) FESEM image of OSLAg.

potential before aging (−50 mV) was increased (to −40 mV) after OSLAg formation (after overnight aging). A decrease in negative zeta potential indicated the formation of zero-valent Ag after nanoparticle formation. The negative charge density was a little decreased due to the conversion of Ag^{+} to Ag^{0}. The zeta potential of −40 mV of OSLAg was high enough to stabilize the silver hydrosol.[1] It is to be noted that the zeta potential was not the sole factor for the stability of the hydrosol. Steric stabilization, depletion (including kinetic interaction, specific adhesion, and specific contact), and delayed aggregation are crucial to nanoparticle stability.[9,32,33] The hydrodynamic diameter of 208.6 nm (polydispersity index 5.7%, mean intensity 324.9 kcps, diffusion coefficient 2.4 $\mu m^2\ s^{-1}$) (before aging) was decreased to 64.5 nm (polydispersity index 27.7%, mean intensity 301.34 kcps, diffusion coefficient 7.6 $\mu m^2\ s^{-1}$) after OSLAg formation (after overnight aging). Thus, the overnight aging of the reaction mixture generated smaller silver nanoparticles with MEF. The FESEM and TEM images also indicated the size of the spherical nanoparticles of OSLAg was ∼60 nm (Fig. 2). The XRD pattern indicated that silver was in a zero-oxidation state in OSLAg (JCPDS file no. 04-0783). The noted 2θ values of 38.36°, 44.6°, 64.56°, and 77.7°, respectively, supported the zero-valent Ag nanoparticles' (111), (200), (210), and (311) planes[34,35] Using Debye–Scherrer's equation $D = 0.9\lambda/\beta\cos\theta$ (where D is the crystalline size, λ is the X-ray wavelength, β is the full width at half maximum of the diffraction peak, and θ is the Bragg's angle), the size of the Ag nanoparticles was determined. Based on the width of the reflection planes, the size of the produced Ag nanoparticles was estimated to be around 14.8 nm.[36]

The lattice fringe of 0.48 nm observed in the HRTEM image was in accord with the (111) plane of zero-valent silver (Fig. 3).[37]

Sensing of gallic acid based on turn-off fluorescence

The strong fluorescence of OSLAg was efficiently decreased by the inclusion of GAc in OSLAg. No other competitive molecules (Zn^{2+}, Na^{+}, K^{+}, Mg^{2+}, succinic acid, citric acid, ascorbic acid, urea, fructose, gallic acid) could quench the fluorescence efficiently, unlike GAc. Such selectivity prompted us to design a fluorometric sensing platform for GAc. The limit of detection (LOD) was 1.77×10^{-5} M while the linear detection range was 10^{-8} to 5×10^{-5} M (Fig. 4). Here, 2 mL of OSLAg and 1 mL of GAc of various concentrations were mixed thoroughly, aged for ∼0.5 h, and the fluorescence spectra then recorded. We calculated LOD values using the slope obtained in the linear detection range. We fitted the data using Excel software and used the LOD formula below to calculate the LOD using the experimental data:

$$\mathrm{LOD} = 3\sigma/s$$

where σ and s represent the calibration curve's slope and the standard deviation, respectively.[38]

Fluorescence quenching refers to any process that decreases the fluorescence intensity of a material. A variety of molecular interactions can result in quenching. These include excited-state

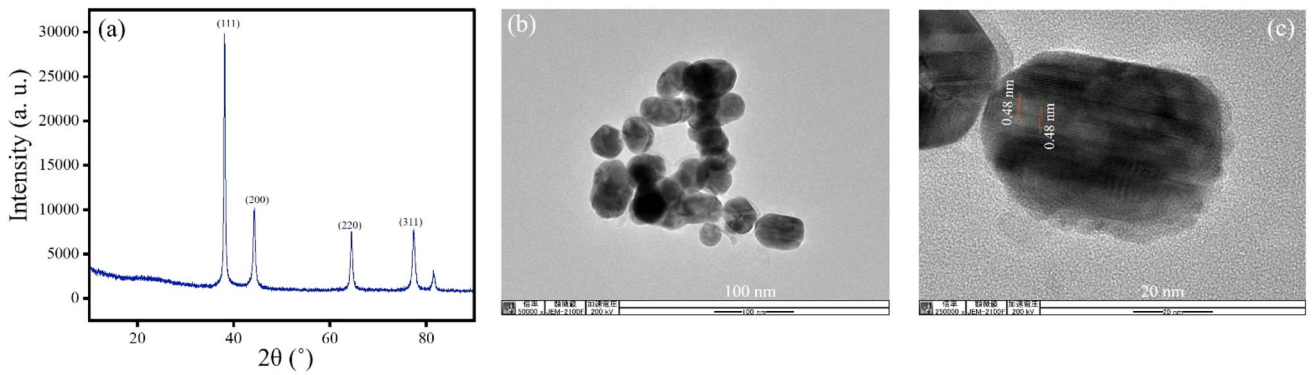

Fig. 3 (a) XRD pattern, (b) TEM image and (c) HRTEM image of OSLAg.

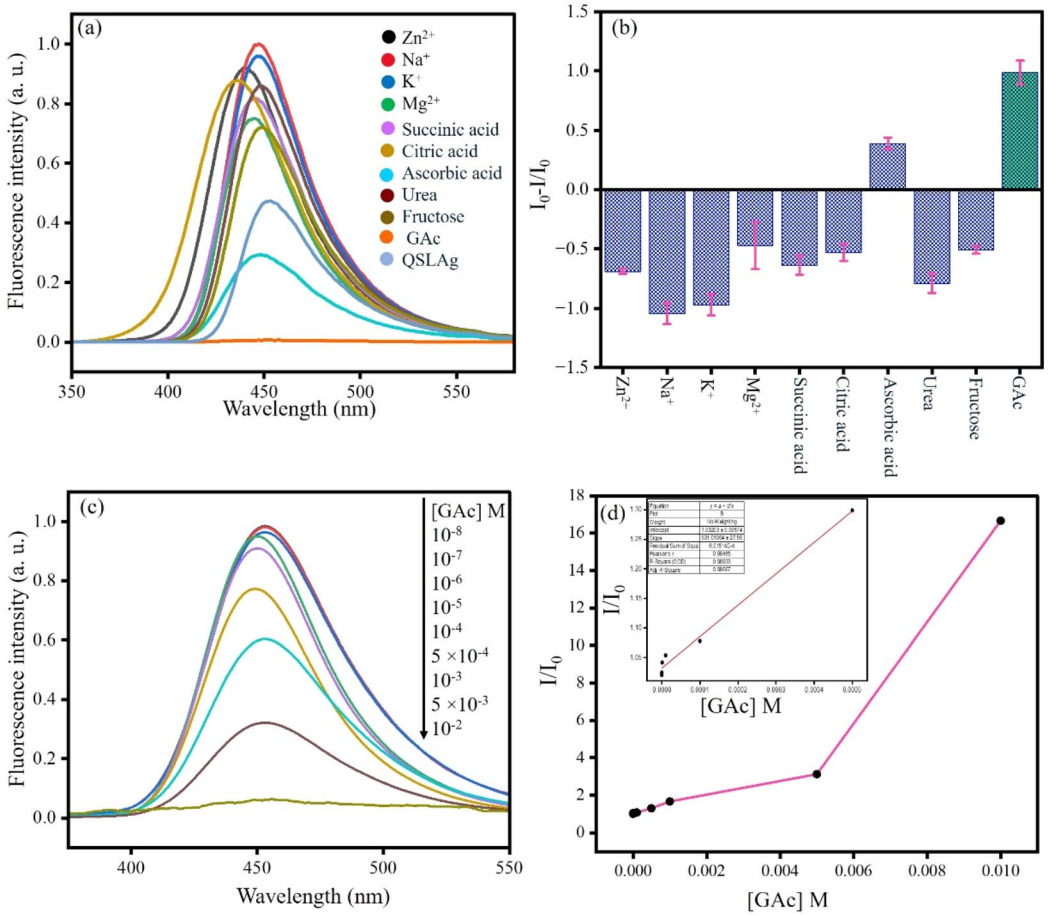

Fig. 4 (a) Emission spectra of OSLAg in the presence of different metal ions. (b) Bar diagram of $I_0 - I/I_0$ for different metal ions. (c) Emission spectra of OSLAg with different [GAc]. (d) Plot of I/I_0 *vs.* [GAc]; inset shows the linear detection range for GAc detection.

reactions, molecular rearrangements, energy transfer, ground-state complex formation, and collisional quenching. Quenching can be induced by different mechanisms, which are usually classified into dynamic quenching and static quenching. Dynamic, *i.e.*, collisional quenching, occurs for excited-state fluorophores.[39]

$$\frac{I_0}{I} = 1 + k_q \tau_0 [Q] = 1 + K_{SV}[Q]$$

Quenching data are usually presented as plots of I_0/I *versus* $[Q]$. This is because I_0/I is expected to be linearly dependent on the concentration of the quencher. A plot of I_0/I *versus* $[Q]$ yields a slope equal to the Stern–Volmer quenching constant K_{SV}. A linear Stern–Volmer plot is generally indicative of a single class of fluorophores, all equally accessible to the quencher. In many cases, the fluorophore can be quenched both by collision and by complex formation with the same quencher. When this is the case, the Stern–Volmer plot exhibits an upward curvature, concave toward the y-axis at high $[Q]$.[39]

The Stern–Volmer plot in our present study showed an upward curvature, implying that both static and dynamic quenching mechanisms were operative. At a lower concentration range (10^{-8} to 5×10^{-5} M), a linear transformer plot was observed with $K_{SV} = 531$ (Fig. 4).

We summarized some different methods and parameters for sensing reported in the available literature in Table 1 in comparison with the present work. Using fluorometric sensing techniques, several research teams have investigated various nanostructures for the detection of GAc. Tan *et al.*[40] developed a fluorescent sensor for the detection of GAc based on the reversible "off–on" fluorescence change of *N*-acetyl-L-cysteine-capped CdTe QDs, with $KMnO_4$ utilized to effectively quench the fluorescence intensity of the QDs. In this kind of sensing, the QDs' fluorescence is first quenched, turned off, and then recovered, or turned on, in the subsequent analyte sequence step. In the light-switching process, this offers the benefits of high selectivity and versatility. The synthesis method though for the QDs was difficult in comparison to our method. Specifically, in their method, the hydrothermal method with modification and N_2 as a protective gas were used for synthesis of the QDs, whereas our synthesis involved a single step only, and no additional reducing agent was required. Zhang *et al.*[41] also reported needing many steps for the synthesis of nanoparticles@zeolitic imidazolate frameworks as a fluorescent nanoprobe.

For the detection of cadmium, a fast, dependable, and extremely sensitive sensor is required.[42] According to recent developments, extremely luminous metal nanoclusters can be expertly created inside biocompatible scaffolds. Using

Table 1 Previously reported nanostructures for the detection of GAc and Cd^{2+}

	Nanoparticles	Method of sensing	LOD for GAc	Detection range
GAc	*N*-Acetyl-L-cysteine-carbon dots[40]	Fluorometric	0.56 ng mL^{-1}	0.6–12.6 μg mL^{-1}
	Carbon dots[45]	Fluorometric	1.2 μmol L^{-1}	2.0–60.0 μmol L^{-1}
	Nanoparticles@zeolitic imidazolate frameworks[41]	Fluorometric	0.35 μM	0–30 μM
	Bovine serum albumin-gold/silver nanoclusters[46]	Fluorometric	45.27 nM	1.25–40.0 μM
	Present study	Fluorometric	1.77×10^{-5} M	10^{-8} to 5×10^{-5} M
	Octamethoxy resorcin[4]arene tetrahydrazide-silver nanoparticles[43]	Fluorometric	10^{-8} M	10^{-8} M to 10^{-6} M
Cd^{2+}	1,13-Bis(8-quinolyl)-1,4,7,10,13-pentaoxatridecane-silver nanoparticles[44]	Colorimetric	2.0 μM	0.5–6.0 μM
	Sulfosalicylic acid-silver nanoparticles[47]	Colorimetric	3.0 nM	0.05–1.1 μM
	Present study	Fluorometric	2.4×10^{-6} M	5×10^{-8} to 10^{-6} M

octamethoxy resorcin[4]arene tetrahydrazide (OMRTH) as a reducing and stabilizing agent, Makwana *et al.*[43] reported the straightforward production of fluorescent Ag nanoparticles. They also reported that Cd^{2+} could quench the emission of the stable silver nanoparticles sensitively and selectively.[43] For the determination of Cd^{2+}, Fallahi and Khayatian[44] suggested a straightforward, quick, and sensitive colorimetric technique, using 1,13-bis(8-quinolyl)-1,4,7,10,13-pentaoxatridecane-modified AgNPs. We believe the reported nanostructures given in Table 1 as sensing platforms are too expensive for cadmium sensing. Moreover, we disclosed here turn-on fluorescence for Cd^{2+} involving silver nanoparticles, unlike in the existing literature.

GAc is an aromatic organic molecule with three phenolate groups. Herein, GAc was oxidized to its quinone[48] form (OGAc) in the reaction mixture. OGAc replaced the capping of OSL on the surface of Ag. Fluorescence was quenched due to the lack of a fluorophore (OSL) in the proximity of the silver nanoparticles surface. Thus, GAc quenched MEF selectively due to the structural parity of OGAc and OSL (Scheme 1).

The zeta potential of OSLAg + OGAc was found to be −28.8 mV and the hydrodynamic diameter (obtained from DLS

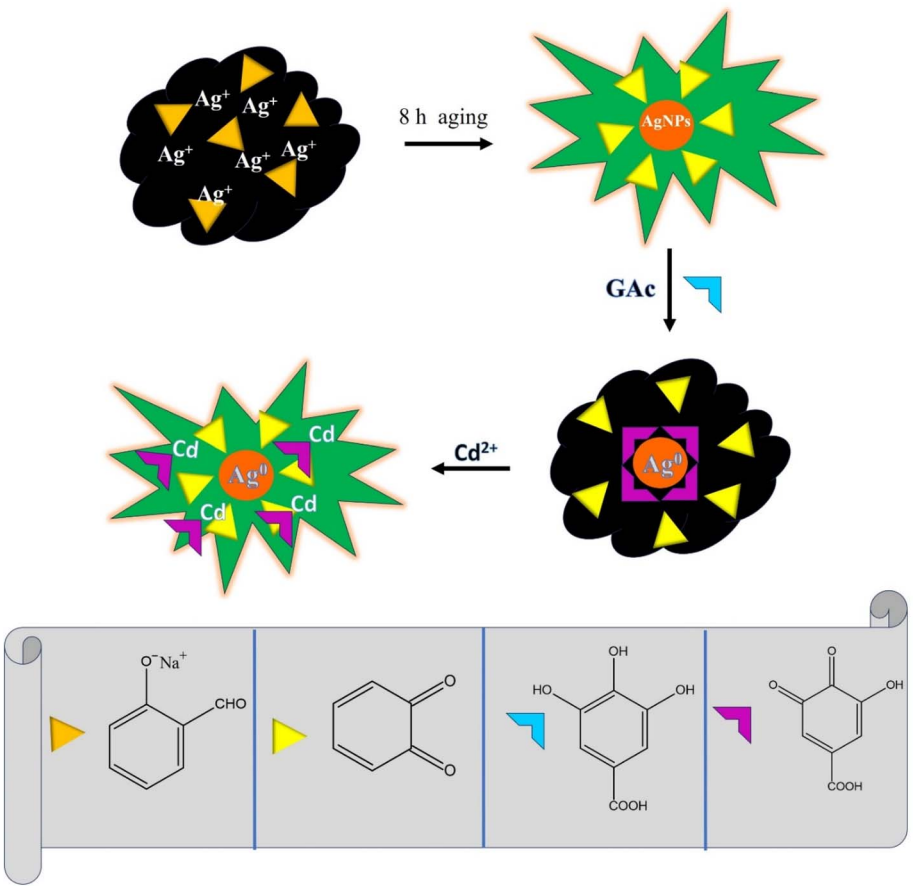

Scheme 1 Mechanistic illustration of gallic acid and Cd^{2+} sensing.

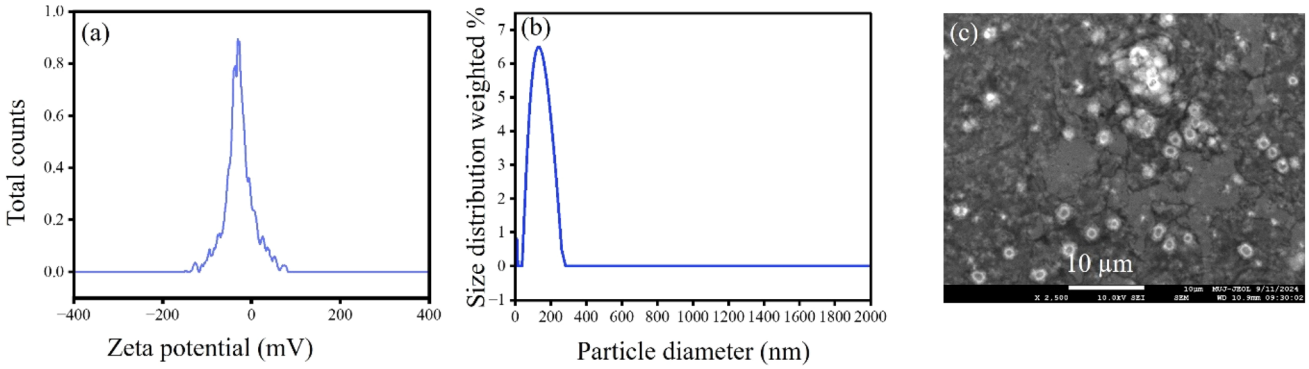

Fig. 5 (a) Zeta potential, (b) DLS plot and (c) FESEM image of OSLAg + OGAc.

analysis) was 112.4 nm. FESEM image also indicated an organic coating on silver nanoparticles and showed that the particles were aggregated due to this coating (Fig. 5).

Sensing of Cd^{2+} based on the restoration of fluorescence

To investigate the effect of interference of other species for GAc sensing, we added both organic (L-leucine, glutathione, uric

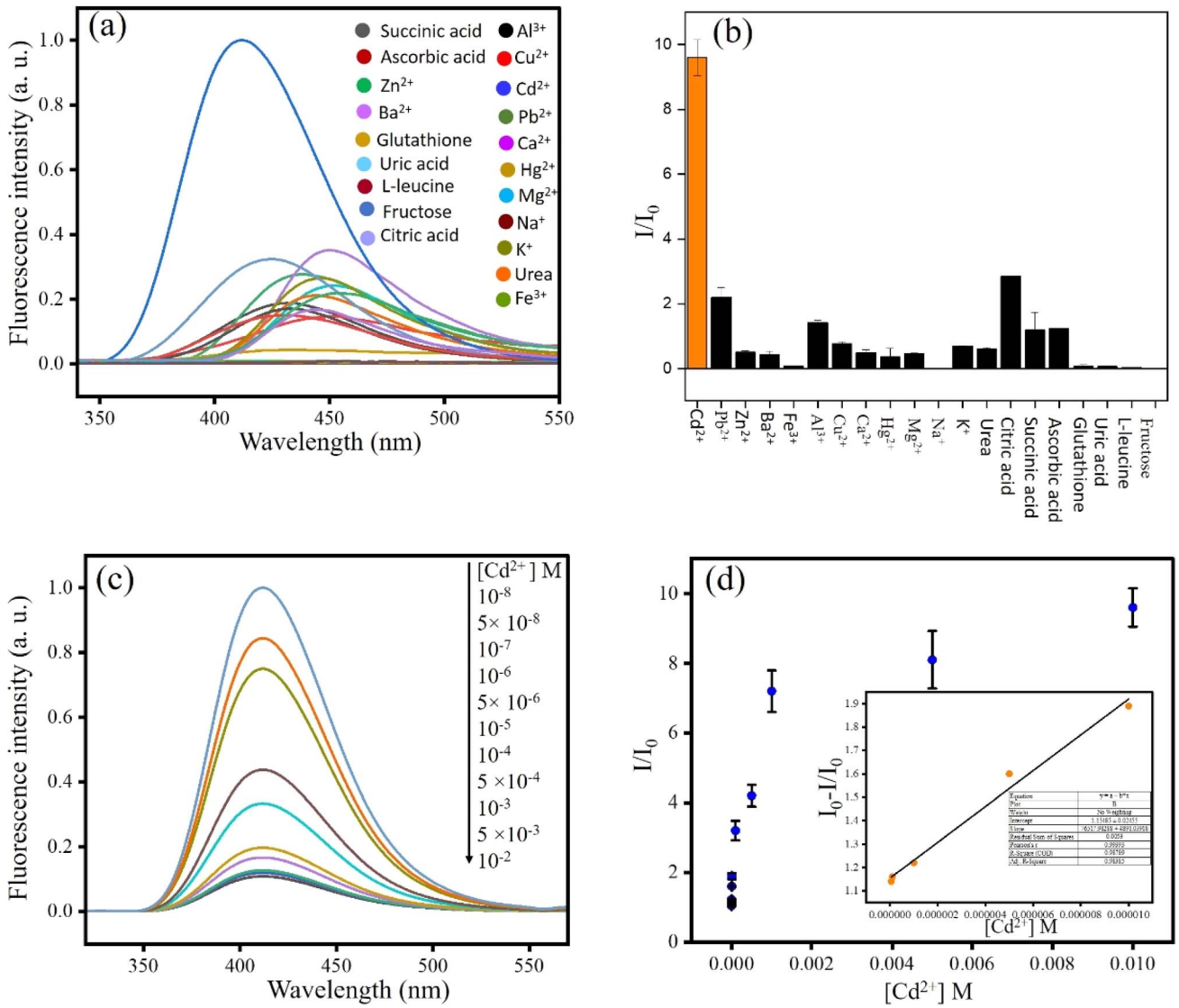

Fig. 6 (a) Fluorescence spectra of OSLAg + OGAc in the presence of various metal ions. (b) Bar diagram of $I_0 - I/I_0$ for different metal ions. (c) Fluorescence spectra of OSLAg + OGAc with different $[Cd^{2+}]$; (d) plot of I/I_0 *vs.* $[Cd^{2+}]$; inset shows the linear detection range for Cd^{2+} detection.

acid, fructose urea, citric acid, succinic acid, ascorbic acid) and inorganic (Cd^{2+}, Pb^{2+}, Cu^{2+}, Zn^{2+}, Ba^{2+}, Fe^{3+}, Al^{3+}, Ca^{2+}, Hg^{2+}, Mg^{2+}, Na^{+}, and K^{+}) materials in OSLAg + OGAc. The quenched fluorescence of OSLAg + OGAc was restored in the presence of Cd^{2+} selectively. No other metal ions could enhance the fluorescence of OSLAg + OGAc. Thus, the Cd^{2+} sensing was made possible with the formation of fluorescent OSLAg + OGAc + Cd^{2+}. The LOD was 2.4×10^{-6} M, while the linear detection range was 10^{-6} to 5×10^{-8} M (Fig. 6). In the experiments, 2 mL of OSLAg, 1 mL of 0.001 M GAc, and various concentrations of Cd^{2+} were mixed thoroughly and aged for 12 h to record the fluorescence spectra.

OSLAg + OGAc + Cd^{2+} had a zeta potential of −46 mV, indicating the high stability of the hydrosol, while the hydrodynamic diameter was found to be 1185 nm. Spherical particles sized ~1 μm were also observed in the FESEM image. In the large spheres, silver particles (white color) remained similar to the eyeballs in the eye (Fig. 7).

Cd^{2+} removed OGAc from the surface of the silver nanoparticles and OSL-capped Ag was regenerated with the restoration of MEF (Scheme 1). The presence of divalent Cd in OSLAg + OGAc + Cd^{2+} was confirmed by XPS analysis and $Cd(OH)_2$ formation was verified. According to the XPS spectra, the peaks at binding energies of 405.01 and 411.73 eV, respectively, matched the divalent cadmium $3d_{5/2}$ and $3d_{3/2}$ states. We did not find peaks for Ag in the XPS survey as Ag was buried by $Cd(OH)_2$ (as confirmed by the FESEM image). The XRD pattern also supported the formation of $Cd(OH)_2$ and Ag_2O (Fig. 8).[49,50] The fluorescence of OSLAg was 1.7 times higher than that of OSLAg + OGAc + Cd^{2+} owing to the surface oxidation of Ag by GAc and Cd^{2+} treatment.

Effect of temperature variation

To test the effects of temperature, we kept OSLAg and OSLAg + OGAc + Cd^{2+} in the chamber of the fluorimeter and varied the

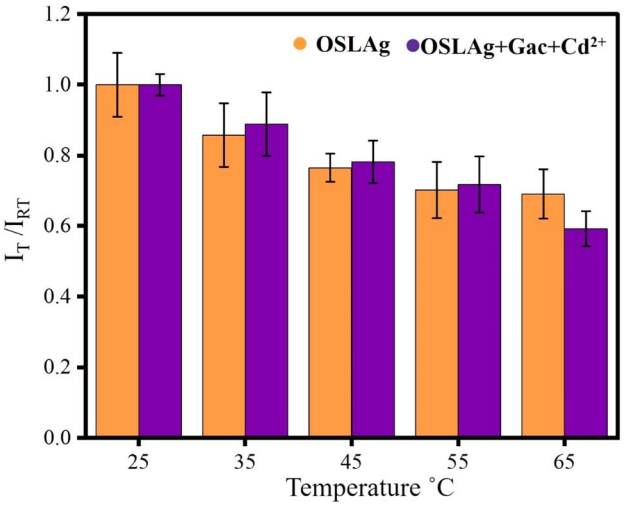

Fig. 9 Fluorescence intensities of OSLAg and OSLAgGAcCd^{2+} at various temperatures with respect to the room temperature.

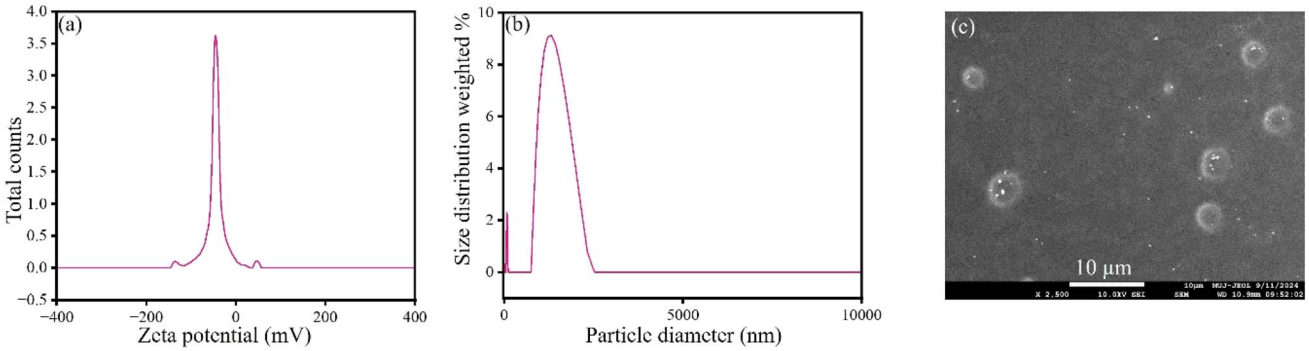

Fig. 7 (a) Zeta potential, (b) DLS plot and (c) FESEM image of OSLAg + OGAc + Cd^{2+}.

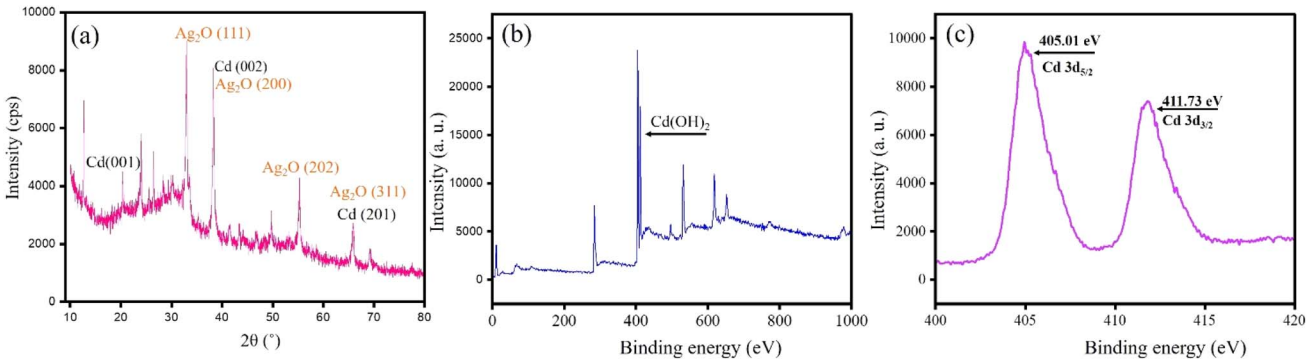

Fig. 8 (a) XRD pattern, (b) XPS survey spectrum, and (c) XPS plot of OSLAg + OGAc + Cd^{2+}.

Table 2 GAc and Cd^{2+} estimation of natural water samples

	Sample	Spiked concentration (M)	Measured (M)	Recovery (%)	RSD ($n = 3$, %)
GAc	Ganga water	3.00×10^{-5}	2.94×10^{-5}	98	3.7
	Rain water	3.00×10^{-5}	3.14×10^{-5}	105	4.1
	Tap water	3.00×10^{-5}	2.75×10^{-5}	92	4.5
Cd^{2+}	Ganga water	3.00×10^{-5}	3.09×10^{-5}	103	1.5
	Rainwater	3.00×10^{-5}	3.12×10^{-5}	104	2.9
	Tap water	3.00×10^{-5}	2.82×10^{-5}	94	2.2

temperature from 25 °C to 65 °C. With the increase in the temperature, fluorescence decreased monotonously for both hydrosols. Increasing Brownian motion was the pivotal factor in the decrease in fluorescence. Energy loss *via* dynamic quenching by the solvent molecules was facilitated by their Brownian motion.[51] However, in the case of OSLAg + OGAc + Cd^{2+}, the reduction in fluorescence was more rapid than that in OSLAg due to the mobility of Cd^{2+} at higher temperatures. Complex formation between Cd^{2+} and OGAc was interrupted at high temperatures. Thus a rapid fluorescence decrement was observed for OSLAg + OGAc + Cd^{2+} due to the joint effect of increased Brownian motion and the increased free quencher [OGAc] at higher temperatures. We plotted I_T/I_{RT} at various experimental temperatures, as shown in Fig. 9 (where I_T and I_{RT} represent the fluorescence intensity at temperature T and room temperature, respectively).

Real sample analysis

In order to assess the viability of the system for practical application, the fluorescence technique mentioned above was used to detect GAc and Cd^{2+} in various natural water samples. We collected Ganga water from Prayagraj (Uttar Pradesh, India), rain water from Jaipur (Rajasthan, India), and tap water from Manipal University Jaipur (India). We filtered the real water samples using Whatman filter paper. We spiked known concentrations of both analytes in three real samples separately to obtain 3.00×10^{-5} M analytes, as mentioned in Table 2. Next, we added the real sample solutions in OSLAg and OSLAgGAc to estimate the [GAc] and [Cd^{2+}] by recording their fluorescence spectra and matching them with their linear detection ranges (Fig. 4 and 6). The added analyte concentrations (known concentrations) and estimated analyte concentrations were found to be close. We checked the calculated % recovery values in Table 2. Though it seems unusual to represent % recovery values >100, it is the way of representation we found in different literature for case % recovery values.[40]

Conclusions

A one-pot sensing platform was designed for gallic acid and Cd^{2+} based on turn-off–turn-on MEF from quinone-capped silver nanoparticles. The observed lightning rod effect and higher rate of radiative decay (due to the high plasmonic density) were ascribed to MEF. Replacement of the capping agents by analytes played a pivotal role in the tuning of MEF in association with nanosensing. For turbid water, the proposed technique has limited applications. Though we anticipate that given the *in situ* formation of orthoquinone, more research is warranted to identify its formation in the aqueous state both theoretically and experimentally. This paper provides a hint on how to tune MEF for nanosensing for many analytes. This paper is expected to be an asset for young scientists venturing into the field of sustainable water management and environmental science.

Data availability

The authors are unable or have chosen not to specify which data have been used.

Author contributions

Mamta Sahu: writing – original draft, Mainak Ganguly: writing – review & editing, conceptualization, Priyanka Sharma: visualization.

Conflicts of interest

The authors declare that they have no known competing financial interests or personal relationships that could have appeared to influence the work reported in this paper.

Acknowledgements

The authors are thankful to Central Analytical Facilities (MUJ) and Sophisticated Analytical Instrument Facility (MUJ) for instrumental facilities.

References

1 S. Dawadi, S. Katuwal, A. Gupta, U. Lamichhane, R. Thapa, S. Jaisi, G. Lamichhane, D. P. Bhattarai and N. Parajuli, Current Research on Silver Nanoparticles: Synthesis, Characterization, and Applications, *J. Nanomater.*, 2021, **2021**, 6687290, DOI: **10.1155/2021/6687290**.

2 C. D. Geddes, Metal-enhanced fluorescence, *Phys. Chem. Chem. Phys.*, 2013, **15**, 19537, DOI: **10.1039/c3cp90129g**.

3 Y. Jeong, Y. M. Kook, K. Lee and W. G. Koh, Metal enhanced fluorescence (MEF) for biosensors: general approaches and a review of recent developments, *Biosens. Bioelectron.*, 2018, **111**, 102–116, DOI: **10.1016/j.bios.2018.04.007**.

4 M. Ganguly, J. Jana, A. Pal and T. Pal, Synergism of gold and silver invites enhanced fluorescence for practical applications, *RSC Adv.*, 2016, **6**, 17683–17703, DOI: 10.1039/c5ra26430h.
5 K. Aslan, I. Gryczynski, J. Malicka, E. Matveeva, J. R. Lakowicz and C. D. Geddes, Metal-enhanced fluorescence: an emerging tool in biotechnology, *Curr. Opin. Biotechnol.*, 2005, **16**, 55–62, DOI: 10.1016/j.copbio.2005.01.001.
6 M. T. Yaraki and Y. N. Tan, Metal Nanoparticles-Enhanced Biosensors: Synthesis, Design and Applications in Fluorescence Enhancement and Surface-enhanced Raman Scattering, *Chem.–Asian J.*, 2020, **15**, 3180–3208, DOI: 10.1002/asia.202000847.
7 S. Pawar, A. Bhattacharya and A. Nag, Metal-Enhanced Fluorescence Study in Aqueous Medium by Coupling Gold Nanoparticles and Fluorophores Using a Bilayer Vesicle Platform, *ACS Omega*, 2019, **4**, 5983–5990, DOI: 10.1021/acsomega.9b00036.
8 L. Y. Jia An, H. Nan and Y. Chengyue, Metal-enhanced fluorescence (MEF) effect based on silver nanoparticles with different UV spectra on a surface carbon dot-based novel dry platform, *Spectrochim. Acta, Part A*, 2024, **322**, 124744.
9 J. Lukomska, J. Malicka, I. Gryczynski, Z. Leonenko and J. R. Lakowicz, Fluorescence enhancement of fluorophores tethered to different sized silver colloids deposited on glass substrate, *Biopolymers*, 2005, **77**, 31–37, DOI: 10.1002/bip.20179.
10 J.-H. Choi and J.-W. Choi, Metal-Enhanced Fluorescence by Bifunctional Au Nanoparticles for Highly Sensitive and Simple Detection of Proteolytic Enzyme, *Nano Lett.*, 2020, **20**, 7100–7107, DOI: 10.1021/acs.nanolett.0c02343.
11 M. Liu, H. Xie, Y. Ma, H. Li, C. Li, L. Chen, B. Jiang and B. Nian, High Performance Liquid Chromatography and Metabolomics Analysis of Tannase Metabolism of Gallic Acid and Gallates in Tea Leaves, *J. Agric. Food Chem.*, 2020, **68**, 4946–4954, DOI: 10.1021/acs.jafc.0c00513.
12 A. Septembre-malaterre, G. Stanislas, E. Douraguia and M. Gonthier, Evaluation of nutritional and antioxidant properties of the tropical fruits banana, litchi, mango, papaya, passion fruit and pineapple cultivated in Réunion French Island, *Food Chem.*, 2016, **212**, 225–233, DOI: 10.1016/j.foodchem.2016.05.147.
13 I. Rahmawati, A. Wedi, S. Abdi, M. Nur, A. Firmanda, F. Haidir, A. Nur, M. Ansori and H. Sucipto, Case studies in chemical and environmental engineering gallic acid: a promising bioactive agent for food preservation and sustainable packaging development, *Case Stud. Chem. Environ. Eng.*, 2024, **10**, 100776, DOI: 10.1016/j.cscee.2024.100776.
14 C. O. Chikere, N. H. Faisal, P. Kong, T. Lin and C. Fernandez, The Synergistic Effect between Graphene Oxide Nanocolloids and Silicon Dioxide Nanoparticles for Gallic Acid Sensing, *J. Solid State Electrochem.*, 2019, **23**, 1795–1809.
15 J. D. Hsu, S. H. Kao, T. T. Ou, Y. J. Chen, Y. J. Li and C. J. Wang, Gallic acid induces G2/M phase arrest of breast cancer cell MCF-7 through stabilization of p27Kip1 attributed to disruption of p27 Kip1/Skp2 complex, *J. Agric. Food Chem.*, 2011, **59**, 1996–2003, DOI: 10.1021/jf103656v.
16 I. Pinchuk, H. Shoval, Y. Dotan and D. Lichtenberg, Evaluation of antioxidants: Scope, limitations and relevance of assays, *Chem. Phys. Lipids*, 2012, **165**, 638–647, DOI: 10.1016/j.chemphyslip.2012.05.003.
17 A. M. Pisoschi, C. Cimpeanu and G. Predoi, Electrochemical Methods for Total Antioxidant Capacity and its Main Contributors Determination: A review, *Open Chem.*, 2015, **13**, 824–856, DOI: 10.1515/chem-2015-0099.
18 H. Zhao, Q. Ran, Y. Li, B. Li, B. Liu, H. Ma, M. Zhang and S. Komarneni, Highly sensitive detection of gallic acid based on 3D interconnected porous carbon nanotubes/carbon nanosheets modified glassy carbon electrode, *J. Mater. Res. Technol.*, 2020, **9**, 9422–9433, DOI: 10.1016/j.jmrt.2020.05.102.
19 W. Ma, D. Han, S. Gan, N. Zhang, S. Liu, T. Wu, Q. Zhang, X. Dong and L. Niu, Rapid and specific sensing of gallic acid with a photoelectrochemical platform based on polyaniline–reduced graphene oxide–TiO_2, *Chem. Commun.*, 2013, **49**, 7842–7844, DOI: 10.1039/c3cc43540g.
20 A. Bernard, Cadmium & its adverse effects on human health, *Indian J. Med. Res.*, 2008, **128**, 557–564.
21 J. Chmielowska-b, J. Gzyl, R. Ruci, M. Arasimowicz-jelonek and J. Deckert, The new insights into cadmium sensing, **5** (2014) 1–14. doi: DOI: 10.3389/fpls.2014.00245.
22 M. Yang, T. J. Jiang, Z. Guo, J. H. Liu, Y. F. Sun, X. Chen and X. J. Huang, Sensitivity and selectivity sensing cadmium(II) using amination functionalized porous SnO_2 nanowire bundles-room temperature ionic liquid nanocomposite: combined efficient cation capture with control experimental conditions, *Sens. Actuators, B*, 2017, **240**, 887–894, DOI: 10.1016/j.snb.2016.09.060.
23 C. ye Hui, Y. Guo, H. Li, C. xian Gao and J. Yi, Detection of environmental pollutant cadmium in water using a visual bacterial biosensor, *Sci. Rep.*, 2022, **12**, 1–11, DOI: 10.1038/s41598-022-11051-9.
24 M. Y. He, Y. J. Lin, Y. L. Kao, P. Kuo, C. Grauffel, C. Lim, Y. S. Cheng and H. H. D. Chou, Sensitive and Specific Cadmium Biosensor Developed by Reconfiguring Metal Transport and Leveraging Natural Gene Repositories, *ACS Sens.*, 2021, **6**, 995–1002, DOI: 10.1021/acssensors.0c02204.
25 S. L. Wang, C. Y. Hsieh, C. R. Wu, J. C. Chen and Y. L. Wang, Highly sensitive FET sensors for cadmium detection in one drop of human serum with a hand-held device and investigation of the sensing mechanism, *Biomicrofluidics*, 2021, **15**, 024110, DOI: 10.1063/5.0042977.
26 M. Sahu, M. Ganguly and P. Sharma, Role of silver nanoparticles and silver nanoclusters for the detection and removal of Hg(II), *RSC Adv.*, 2024, **14**, 22374–22392, DOI: 10.1039/d4ra04182h.
27 M. Ganguly, J. Pal, C. Mondal, A. Pal and T. Pal, Intriguing Manipulation of Metal-Enhanced Fluorescence for the Detection of CuIIand Cysteine, *Chem.–Eur. J.*, 2014, **20**, 12470–12476, DOI: 10.1002/chem.201402505.
28 M. Sahu, M. Ganguly, P. Sharma, A. Doi and Y. Negishi, Simultaneous ionic cobalt sensing and toxic Congo red dye

removal: a circular economic approach involving silver-enhanced fluorescence, *Nanoscale Adv.*, 2024, **6**, 6173–6183, DOI: 10.1039/d4na00588k.

29 J. R. Lakowicz, Y. Shen, S. D'Auria, J. Malicka, J. Fang, Z. Gryczynski and I. Gryczynski, Radiative decay engineering: 2. Effects of silver island films on fluorescence intensity, lifetimes, and resonance energy transfer, *Anal. Biochem.*, 2002, **301**, 261–277, DOI: 10.1006/abio.2001.5503.

30 M. Sahu, M. Ganguly and A. Doi, Metal-Enhanced Fluorescence due to Salicylaldehyde-Silver Nanoparticle Interactions for Fe^{3+} Sensing, *ChemistrySelect*, 2023, **8**, e202301017, DOI: 10.1002/slct.202301017.

31 J. Jana, M. Ganguly and T. Pal, Evolution, Stabilization, and Tuning of Metal-Enhanced Fluorescence in Aqueous Solution, *Surface Plasmon Enhanced, Coupled and Controlled Fluorescence*, 2017,pp. 151–178, doi: DOI: 10.1002/9781119325161.ch9.

32 P. Sharma, M. Ganguly and M. Sahu, Na^+ detection *via* brightening of synergistically originated noble metal nanoclusters, *RSC Adv.*, 2024, **14**, 31624–31632, DOI: 10.1039/d4ra05501b.

33 P. Attard, Recent advances in the electric double layer in colloid science, *Curr. Opin. Colloid Interface Sci.*, 2001, **6**, 366–371, DOI: 10.1016/S1359-0294(01)00102-9.

34 M. Sahu, M. Ganguly and P. Sharma, Recent applications of coinage metal nanoparticles passivated with salicylaldehyde and salicylaldehyde-based Schiff bases, *Nanoscale Adv.*, 2024, **6**, 4545–4566, DOI: 10.1039/d4na00427b.

35 M. Sahu, M. Ganguly and P. Sharma, Fluorescent Giant Clusters with Myriad Applications, *NanoWorld J.*, 2023, **9**, 496–504, DOI: 10.17756/nwj.2023-s5-080.

36 Y. Meng, A Sustainable Approach to Fabricating Ag Nanoparticles/PVA Hybrid Nanofiber and Its Catalytic Activity, *Nanomaterials*, 2015, **5**, 1124–1135, DOI: 10.3390/nano5021124.

37 N. A. Bakar, J. G. Shapter, M. M. Salleh and A. A. Umar, Self-Assembly of high density of triangular silver nanoplate films promoted by 3-aminopropyltrimethoxysilan, *Appl. Sci.*, 2015, **5**, 209–221, DOI: 10.3390/app5030209.

38 J. Li, B. Zheng, Z. Zheng, Y. Li and J. Wang, Highly sensitive and selective colorimetric and SERS dual-mode detection of arsenic (III) based on glutathione functionalized gold nanoparticles, *Sens. Acutators Rep.*, 2020, **2**, 100013, DOI: 10.1016/j.snr.2020.100013.

39 J. Mariam, P. M. Dongre and D. C. Kothari, Study of Interaction of Silver Nanoparticles with Bovine Serum Albumin Using Fluorescence Spectroscopy, *J. Fluoresc.*, 2011, **21**, 2193–2199, DOI: 10.1007/s10895-011-0922-3.

40 X. Tan, Q. Li and J. Yang, CdTe QDs based fluorescent sensor for the determination of gallic acid in tea, *Spectrochim. Acta, Part A*, 2020, **224**, 117356, DOI: 10.1016/j.saa.2019.117356.

41 Y. Zhang, L. Ning, D. Gao, D. Jia, W. Gu and X. Liu, A highly sensitive upconversion nanoparticles@zeolitic imidazolate frameworks fluorescent nanoprobe for gallic acid analysis, *Talanta*, 2021, **233**, 122588, DOI: 10.1016/j.talanta.2021.122588.

42 S. Velanki, S. Kelly, T. Thundat, D. A. Blake and H. Ji, Detection of Cd(II) using antibody-modified microcantilever, *Sensors*, 2007, **107**, 1123–1128, DOI: 10.1016/j.ultramic.2007.01.011.

43 B. A. Makwana, D. J. Vyas, K. D. Bhatt, S. Darji and V. K. Jain, Novel fluorescent silver nanoparticles: sensitive and selective turn off sensor for cadmium ions, *Appl. Nanosci.*, 2016, **6**, 555–566, DOI: 10.1007/s13204-015-0459-x.

44 M. R. Fallahi and G. Khayatian, Cadmium determination based on silver nanoparticles modified with 1,13-bis(8-quinolyl)-1,4,7,10,13-pentaoxatridecane, *J. Iran. Chem. Soc.*, 2017, **14**, 1469–1476, DOI: 10.1007/s13738-017-1087-z.

45 X. H. Qin Tan, X. An, S. Pan, S. Zhen and Y. Hu, A facile and sensitive ratiometric fluorescent sensor for determination of gallic acid, *Microchem. J.*, 2022, **172**, 106922.

46 M. Wang, Z. Liu, M. Wu, T. Wong, X. Yu, N. Niu and L. Chen, Ratiometric luminescent sensor based on BSA-coated gold/silver nanoclusters for the selective determination and spatiotemporal imaging of gallic acid in plants, *Microchim. Acta*, 2024, **191**, 60.

47 W. Jin, P. Huang, F. Wu and L. H. Ma, Ultrasensitive colorimetric assay of cadmium ion based on silver nanoparticles functionalized with 5-sulfosalicylic acid for wide practical applications, *Analyst*, 2015, **140**, 3507–3513, DOI: 10.1039/c5an00230c.

48 G. Ziyatdinova, E. Guss, E. Morozova, H. Budnikov, R. Davletshin, V. Vorobev and Y. Osin, Simultaneous voltammetric determination of gallic and ellagic acids in cognac and brandy using electrode modified with functionalized SWNT and poly(pyrocatechol violet), *Food Anal. Methods*, 2019, **12**, 2250–2261, DOI: 10.1007/s12161-019-01585-6.

49 L. A. Saghatforoush, S. Sanati, R. Mehdizadeh and M. Hasanzadeh, Solvothermal synthesis of $Cd(OH)_2$ and CdO nanocrystals and application as a new electrochemical sensor for simultaneous determination of norfloxacin and lomefloxacin, *Superlattices Microstruct.*, 2012, **52**, 885–893, DOI: 10.1016/j.spmi.2012.07.019.

50 Y. C. Zhang and G. L. Wang, Solvothermal synthesis of CdO hollow nanostructures from CdO_2 nanoparticles, *Mater. Lett.*, 2008, **62**, 673–675, DOI: 10.1016/j.matlet.2007.06.031.

51 M. Ganguly, A. Pal, Y. Negishi and T. Pal, Diiminic Schiff bases: an intriguing class of compounds for a copper-nanoparticle-induced fluorescence study, *Chem.–Eur. J.*, 2012, **18**, 15845–15855, DOI: 10.1002/chem.201201242.